Available online at www.sciencedirect.com
ScienceDirect
Journal of Power Sources 158 (2006) 851–863
JOURNAL OF POWER SOURCES
www.elsevier.com/locate/jpowsour

Graphite and fiberglass additives for improving high-rate partial-state-of-charge cycle life of valve-regulated lead-acid batteries

J. Valenciano [a,*], A. Sánchez [a], F. Trinidad [a], A.F. Hollenkamp [b]

[a] *Research & Innovation Center, Exide Technologies, Autovía A-2, Km 42, E-19200 Azuqueca de Henares, Spain*
[b] *CSIRO Energy Technology, Bayview Avenue, Clayton, Vic. 3168, Australia*

Available online 27 December 2005

Abstract

In order to accommodate regenerative braking energy input in hybrid and mild hybrid vehicles while maintaining boosting power at high rates of discharge, valve-regulated lead-acid (VRLA) batteries must operate permanently at partial-state-of-charge (PSoC) conditions. As a consequence, new failure modes appear, e.g., irreversible sulfation in negative plates, that have to be overcome.

In this way, work has been done to apply some solutions like improving charge acceptance in this "sulfated medium". Several batches of 6 V 20 Ah AGM VRLA batteries with spiral cell design have been assembled and tested, each batch containing novel additives in the negative active material (NAM). It has been observed that the addition of a sufficient amount of expanded graphite significantly improves cycle life under PSoC conditions. Moreover, life duration is also extended, although to a lesser extent, by using a novel fiberglass which increases surface area of NAM.

Keywords: Fiberglass; Graphite; High-rate partial-state-of-charge; Irreversible sulfation; Spiral-wound; Valve-regulated lead-acid

1. Introduction

Batteries working under hybrid electric vehicle (HEV) service are exposed to a duty cycle which is quite different from any other function that lead-acid batteries have been required to perform. The batteries operate at partial-state-of-charge (PSoC) rather than from a fully charged condition, and charges and discharges tend to be of short duration but high rate.

Under these conditions, lead-acid batteries which have been designed for conventional tasks (e.g., SLI or deep cycle), fail rather quickly due to sulfation of negative plates. In order to adapt valve-regulated lead-acid (VRLA) batteries to perform the function required in HEVs (e.g., for accommodating regenerative braking energy input while maintaining boosting power at high rates of discharge), several studies have been carried out to overcome these new failure modes [1], i.e., progressive accumulation of lead sulfate mainly on the surfaces of the negative plates whereas positive plates remain healthy. Lead sulfate cannot be converted efficiently back to sponge lead during regenerative braking charging. Eventually, the lead sulfate layer develops to such extent that the effective surface area of the plate is reduced markedly and the plate can no longer deliver the high cranking-current demanded by the automobile. During high-rate partial-state-of-charge (HRPSoC) duty, high rate discharge is the key factor responsible for the build-up of a compact layer of lead sulfate crystals on the surface of the negative plate, and subsequent charging gives rise to an early evolution of hydrogen. Hydrogen evolution is further exacerbated when a high charging current is used. However, by adjusting the type and loading of carbon materials, a significant increase of HEV cycle life has been achieved [2]. It appears that carbon materials used in negative plates destined for HRPSoC exert a beneficial effect by: (i) maintaining a conductive network through the negative plate material, especially at low states-of-charge and (ii) increasing the effective electrode surface area of the plate.

2. Experimental

In this way, work has been done to implement some of the potential solutions above-mentioned for increasing the performance of negative plates that, otherwise under HRPSoC conditions, become rapidly and progressively sulfated, i.e., by adding novel additives to increase conductivity

* Corresponding author. Tel.: +34 949 263 316; fax: +34 949 262 560.
E-mail addresses: valencianoj@tudor.es (J. Valenciano), sancheza@tudor.es (A. Sánchez), trinidadf@tudor.es (F. Trinidad), Tony.Hollenkamp@csiro.au (A.F. Hollenkamp).

0378-7753/$ – see front matter © 2005 Published by Elsevier B.V.
doi:10.1016/j.jpowsour.2005.11.058

Table 1
Experimental matrix and parameter design

Batch no.	PAM density (g cm^{-3})	NAM density (g cm^{-3})	Organic expander (%)	Carbon (%)	Inorganic additive (%)
1	4.3	4.3	0.2	0.2 CB	–
2	4.3	4.3	0.3	0.2 CB	–
3	4.3	4.3	0.2	1.5 EG	–
4	4.3	4.3	0.2	1.5 FG	–
5	4.3	4.3	0.2	1.5 FG	1.5 micro-fiberglass
6	4.0	4.3	0.2	1.5 EG	–

CB: standard carbon black (used in current plant production); higher amount of organic expander (0.3% vs. 0.2%); EG: expanded graphite (high SSA = 24 m^2 g^{-1}); FG: flake graphite (low SSA = 9 m^2 g^{-1}); micro-fiberglass + FG; lower density in PAM (4.0 g cm^{-3} vs. 4.3 g cm^{-3}), EG in NAM.

as well as specific surface area (SSA) of negative active material (NAM).

Several batches of 6 V 20 Ah High Power AGM VRLA batteries [3] with spirally wound cells and deep cycling formulation in positive active material (PAM) have been manufactured at Exide's Zaragoza plant using the current production line, each batch containing the negative active material composition set forth in Table 1. This spiral cell design together with the specific PAM cycling formulation allow to maintain compression on positive electrode along cycle life. In addition, the cylindrical cell is an ideal shape for allowing space between cells for an adequate battery thermal management [4].

Two different carbon materials (expanded graphite and flake graphite) have been included in the study. Both of them show similar conductive properties, but with different surface area to see the influence of this parameter in cycle life at PSoC. The expanded graphite has been previously used by our group showing a positive effect in extending cycle life of AGM VRLA high power prismatic batteries [5].

The control batch (Batch 1) was manufactured with the carbon black type and loading used in the current plant production. Additionally, one batch of prototypes with a novel micro-fiberglass that was claimed to increase SSA of negative active material [6] has been tested together with the low SSA graphite. To complete the experimental matrix, the influence of organic expander (lignosulfonate) dosage has been also analyzed. Batch 1 has been designed on the basis of knowledge acquired in Brite–Euram Project BE97-4085 (IMPLAB, Task 3: Improvements in Negative Plate Performance) in which 0.2 wt.% organic expander was determined as the optimum concentration, mainly in terms of charge-acceptance performance.

However, due to the emphasis which HRPSoC duty places on high-rate charging characteristics, it has been decided, with Batch 2, to investigate the possible benefits of an increased level of organic expander, viz., 0.3 wt.%. Finally, the contribution of PAM density (Batch 3 versus Batch 6) in an HRPSoC duty has been also investigated.

3. Results and discussion

3.1. Physical properties of NAM

The initial influence of novel additives in newly formed prototypes is shown in Fig. 1. NAMs containing EG as well as micro-fiberglass have increased their SSA (BET values) with respect to the control batch, indicating a first effective action

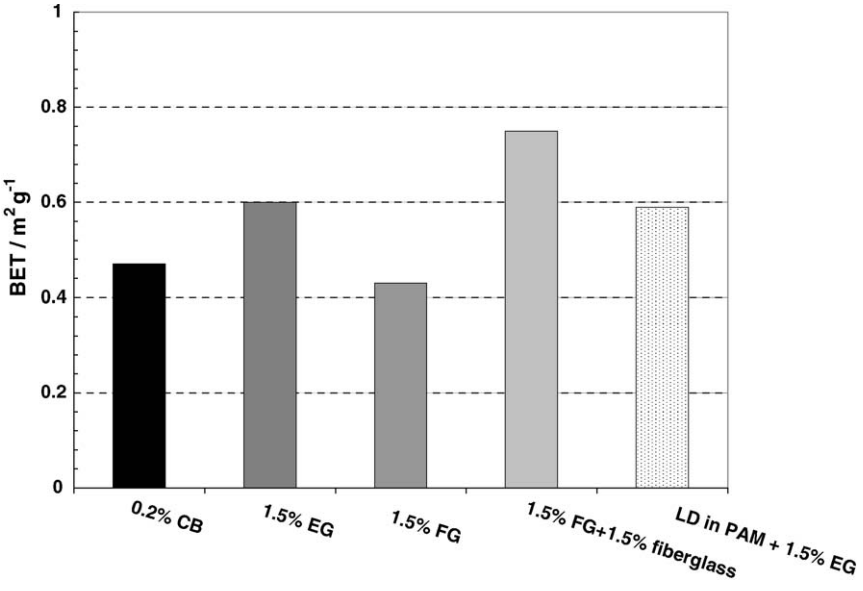

Fig. 1. Specific surface area (BET) of formed NAM.

Table 2
Initial electrical tests on Batches 1–6[a]

	Batch 1	Batch 2	Batch 3	Batch 4	Batch 5	Batch 6
Reserve capacity (25 A to 5.25 V, min)	34.5	32.0	34.0	35.5	34.5	39.0
Capacity (C_{20}) (Ah)	22.9	21.6	22.3	22.4	22.2	24.0
Cold cranking at −18 °C (400 A to 3.6 V, s)	18	21	18	26	22	16

[a] Average of six modules.

of these materials in the key PSoC/HEV properties required for negative plates. Addition of EG increased SSA by 25% in Batches 3 and 6 with respect to the control batch, whereas the use of novel fiberglass has allowed an increase higher than 50% in surface area of negative plates belonging to Batch 5. However, flake graphite alone (Batch 4) gives BET values similar to control batch.

3.2. Electrical characterization

Electrical testing of prototypes was performed with computer controlled cycling equipment: Bitrode LCN-7-100-12 and Digatron UBT 100-60-3 BTS and HEW 2000/12-700/36. High rate discharges were performed with a computer controlled Digatron UBT BTS-500, model HEW 2000-6BTS. After the initial tests (Table 2), the different prototypes were submitted to the selected tests described below, which are included in the specifications developed by EUCAR Traction Battery Working Group for hybrid vehicle and for 42 V applications (1998 and 2003, respectively) [7].

3.2.1. Constant current discharges

Initially, the 6 V batteries were submitted to some initial discharge–charge tests, showing a similar electrical performance, except for modules from Batch 6 which, due to the lower density in PAM, gave higher capacity values both in reserve capacity and 20-h discharge tests.

To establish the discharge performance at different rates, all batches were discharged under constant current conditions at the following rates: 10, 20, 40, 100, 200, 300, 400 and 500 A. The results obtained are represented as Peukert plots in Figs. 2 and 3 below. As shown in the figures, only minor differences are found among the six groups tested, indicating no influence of NAM additives in high rate discharge performance of the modules with different NAM formulations.

Only Batch 6 gave higher capacity values up to 10 C rate when compared with the other groups tested, result that could be explained by the lower density of the positive active material in this batch.

3.2.2. High rate charge and discharge performance at room temperature

As discussed above, high power capability and high rate charge acceptance are important battery features in HEV concepts, as battery is aimed at assisting conventional engines during vehicle acceleration and to store energy from regenerative braking. The peak power and charge acceptance of 36 V prototypes (six 6 V modules in series) have been tested at 25 °C and at different states of charge (SoC), ranging from 100 to 20%. The peak power values were obtained at 400 A, discharging down

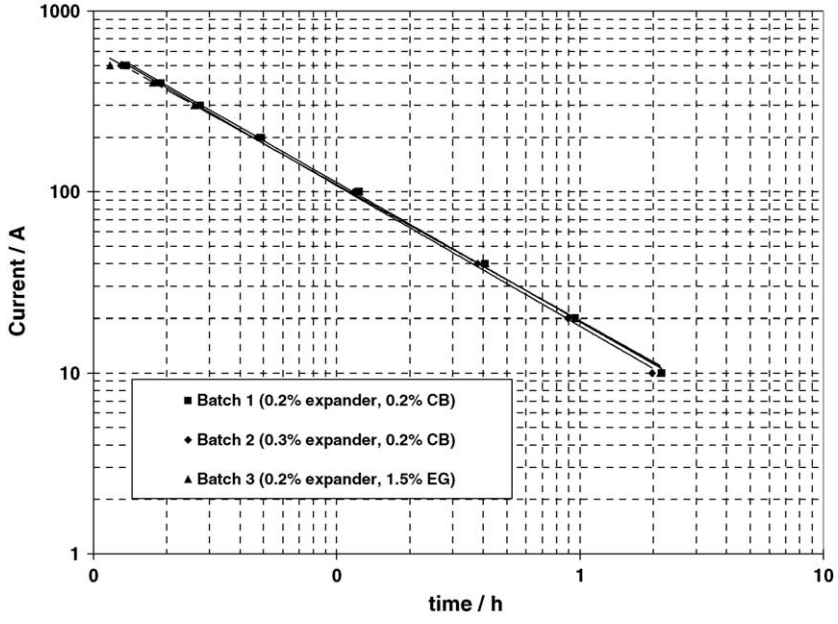

Fig. 2. Peukert curve of Batches 1–3.

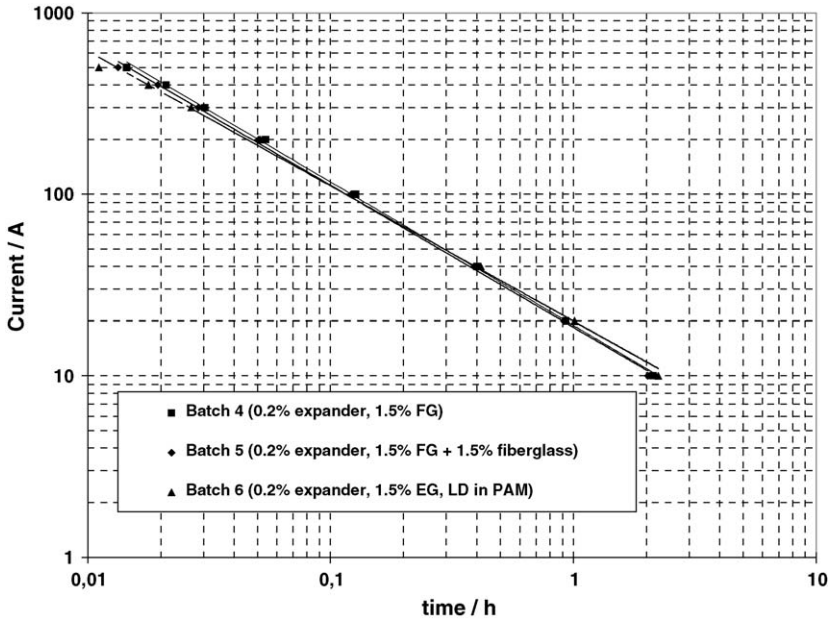

Fig. 3. Peukert curve of Batches 4–6.

to 30 V and in the charge acceptance test the maximum voltage was limited to 48 V.

Generally, the power values at high SOC were similar for the six groups tested (Figs. 4 and 5). Concerning high rate charge acceptance, the following conclusions can be extracted from this test.

Firstly, batteries having a higher expander content (Batch 2) showed a lower charge acceptance than the standard (Batch 1). Secondly, high surface area graphite (expanded) seems to improve charge acceptance in Batches 3 and 6 especially from 80 to 20% SoC (Figs. 4 and 5), whereas the Batch 4 batteries which contained flake graphite alone showed the lowest charge acceptance (Fig. 5). However, the fiberglass additive in Batch 5 improved charge acceptance when compared to Batch 4 (both containing flake graphite), a result that could be ascribed to the higher SSA of the active material (Fig. 1).

3.2.3. *Power assist life cycle test and failure mode analysis*

To check the performance of the batteries under HRPSoC conditions, 6 V modules from each batch were tested according to the EUCAR *Power Assist Life Cycle Test* [7] at 2.5% DoD. The batteries were previously discharged to 60% SoC and then continuously cycled according to the "microcycle" shown in Fig. 6 that simulates the boosting, cruise, regenerative braking and stop periods of an HEV duty cycling. The modules were cooled with forced airflow at 25 °C.

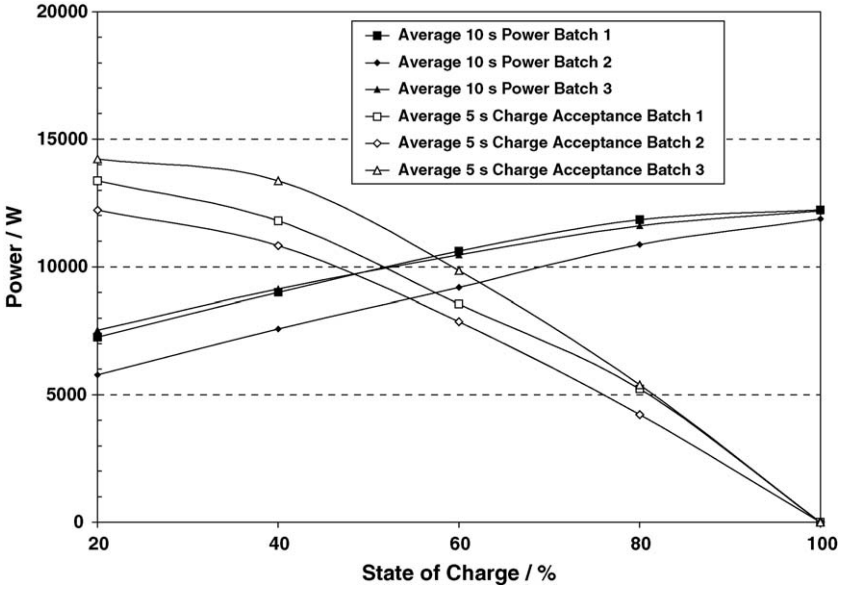

Fig. 4. Power and charge acceptance vs. SoC (Batches 1–3).

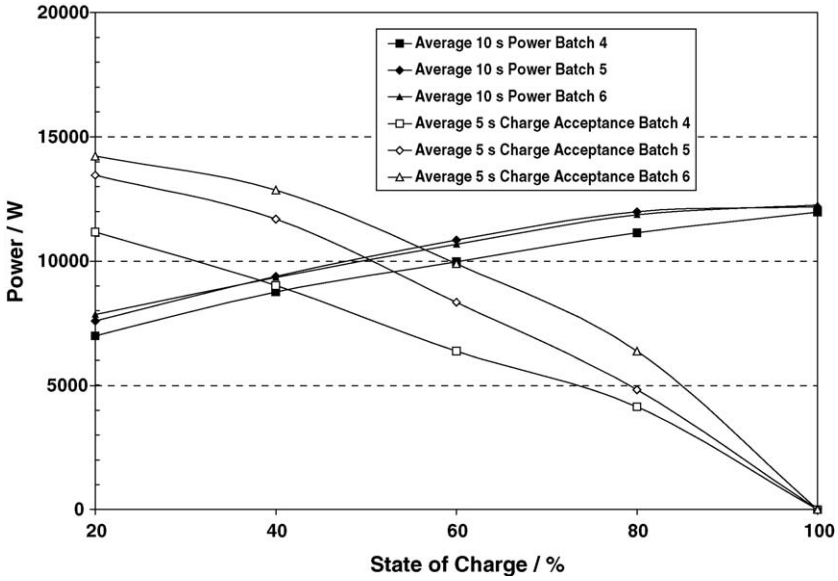

Fig. 5. Power and charge acceptance vs. SoC (Batches 4–6).

Two battery failure criteria have been considered: the voltage in the 5 C discharge drops below 5 V or the control capacity after every 10,000 microcycles is lower than 50% of the initial value.

Several 6 V modules from each batch (labeled as "b" type) were cycled according to the above profile, these prototypes being sealed with rubber plugs in order to have access to the interior of the cells to take measurements of negative plate potential (versus a cadmium reference electrode) during the service life.

Having completed the power assist test for modules from each batch, it is clear that a direct relationship exists between negative plate formulation and number of PSoC cycles fulfilled by each battery type. The following graphs show the evolution of end of discharge voltage (EDV) and internal resistance increase as well as the capacity and weight loss during cycle life. Firstly, the addition of a sufficient amount of expanded graphite (Batches 3 and 6) significantly improved cycle life under PSoC conditions (up to 25% increase with respect to standard formulation), reaching a capacity throughput of 3250. Moreover, life duration was also extended, although to a lesser extent, by using the fiberglass which increases NAM surface area. Batteries with low SSA graphite showed the poorer life performance, supporting a new evidence of the relationship between SSA and PSoC cycle life (Fig. 7).

The positive influence of expanded graphite formulation in NAM can be seen not only in the higher end of discharge voltage during cycling but also in the more steady increase of ac internal resistance measured every 10,000 microcycles for modules containing the novel carbon additive, as set forth in Fig. 8. This indicates that the expanded graphite used improves active material conductivity along life.

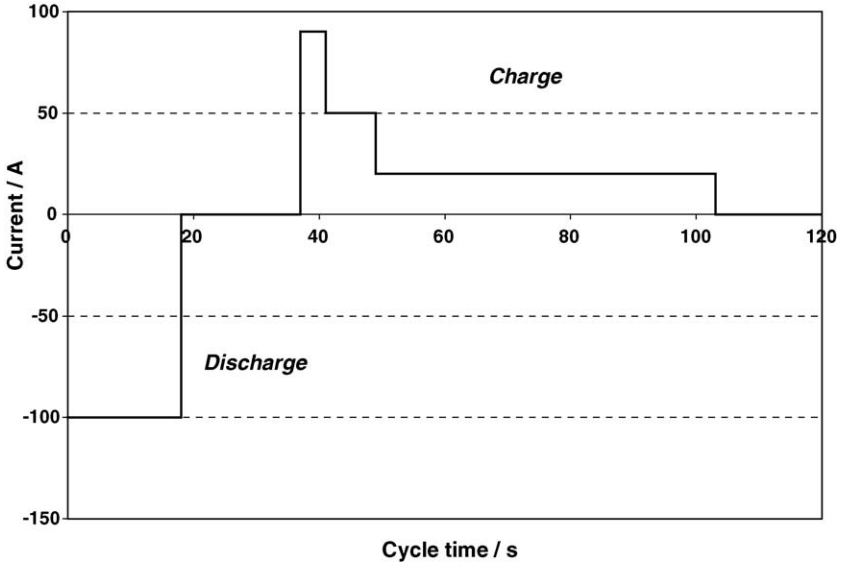

Fig. 6. Power assist life cycle test profile.

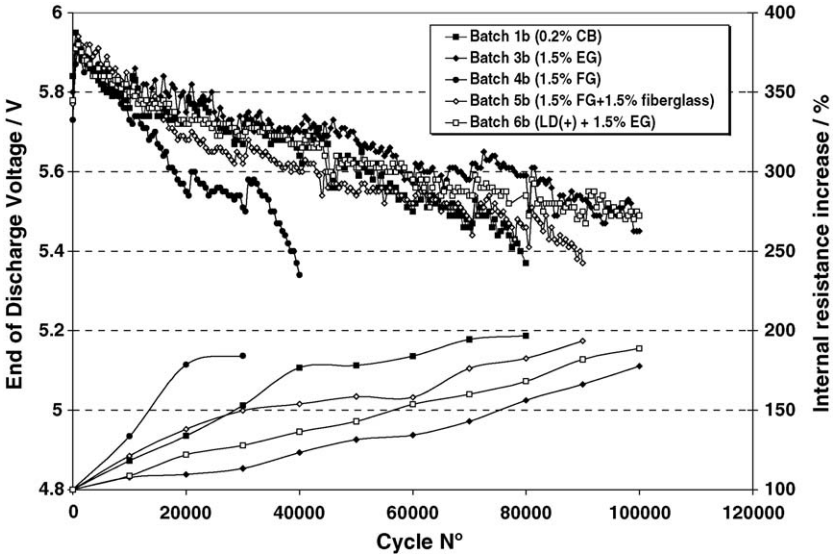

Fig. 7. Number of power assist cycles fulfilled (end of discharge voltage and internal resistance vs. cycle no.).

A direct relationship between remaining capacity and weight loss every 10,000 microcycles can also be observed in Fig. 8, especially for prototypes containing flake graphite (Batch 4).

In order to know which is the limiting electrode according to the power assist profile, some experiments were carried out with rubber-plugged prototypes introducing cadmium reference electrodes in the interior of the cells. Fig. 9 shows the voltage of positive and negative plates of a battery cell belonging to Batch 1b recorded at the end of the life (80,000 cycles). It can be observed a clear increase of end of charge voltage (ECV) of the negative electrode at the end of the charge period, whereas positive electrode voltage remains constant.

These results agree with those the previously reported by CSIRO [1,8]. Although at the beginning of this 8th unit both positive and negative plates showed a voltage drop during the discharge period, from about cycle no. 76,000, the voltage decrease is mainly observed for negative plate. It is worth mentioning that these results correspond to a single cell and the evolution of the other 2 V elements can be somewhat different due to uneven charge and discharge conditions in the cells of the 6 V module.

A second set of tests according to power assist profile were conducted on thermosealed modules (labeled as 1–6), although in this case cadmium measurements were not taken in order not to interfere with the sealed battery system. As it was reported above for "plugged" modules, EDV, internal resistance evolution, capacity and weight loss data were also recorded and presented in Figs. 10 and 11, respectively. In this case a direct comparison between Batches 1 and 2 is obtained, both groups of batteries having fulfilled 110,000 cycles. It is interesting to point

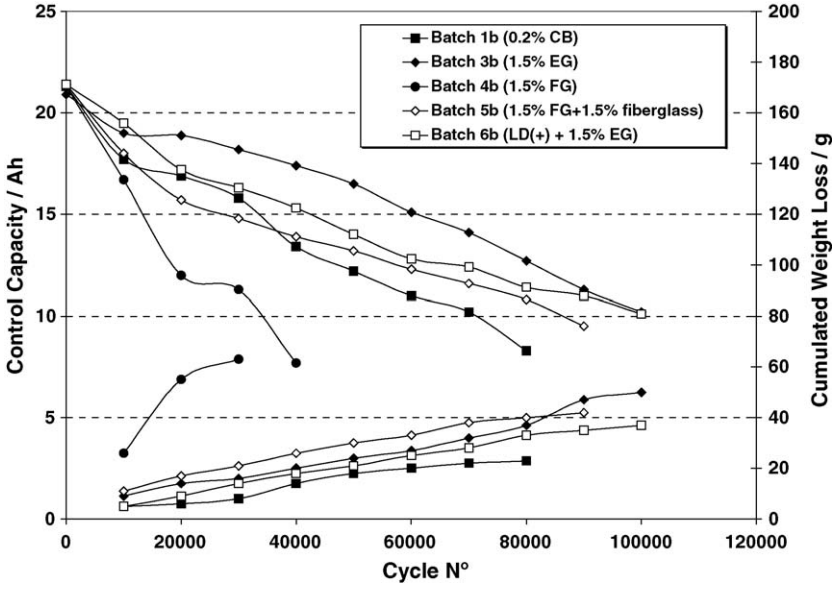

Fig. 8. Number of power assist cycles fulfilled (capacity and weight loss vs. cycle no.).

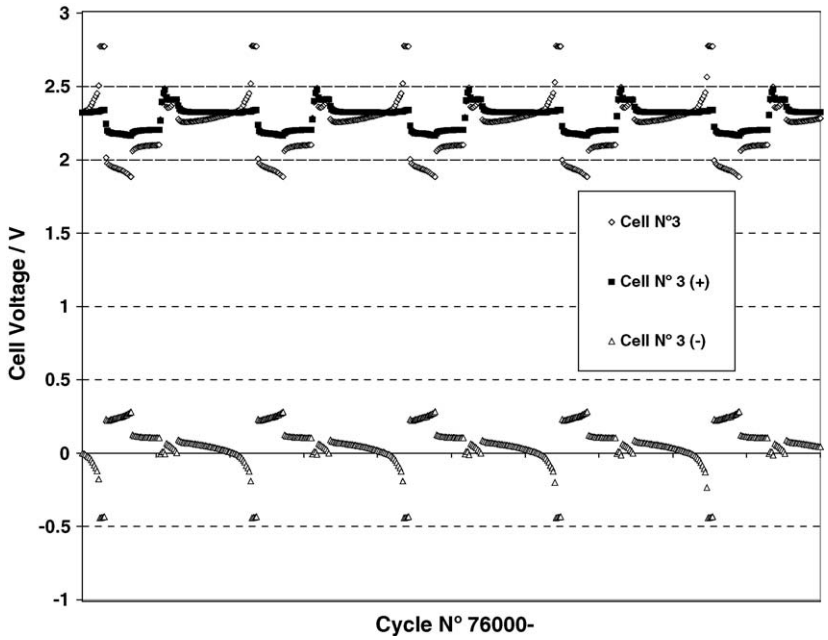

Fig. 9. Cadmium reference electrode measurements at the end of life of a 6 V module belonging to Batch 1b.

out that the expander content (0.2% versus 0.3%, respectively) does not affect PSOC cycle life.

However, the more outstanding performance was obtained with two batteries containing expanded graphite and low density in PAM (Batch 6), which show again a higher performance in terms of EDV and capacity throughout cycling than the rest of the groups (Figs. 10 and 11). In addition, they present a lower internal resistance than the control modules in every 10,000 cycles check (Fig. 10). Therefore, these modules have completed 130,000 and 140,000 modules, respectively, i.e., about 20% increase in cycle life with respect to Batches 1 and 2.

More complex results have been obtained from modules belonging to Batches 3, 4 and 5, since in all cases the batteries completed less than 100,000 cycles, i.e., a shorter life when compared to control modules (Batch 1). With respect to the Batch 3, this result is unexpected as in the tests carried out on "plugged" systems both types of batteries containing expanded graphite (Batches 3b and 6b) showed a longer life compared to control prototypes. Although modules of Batch 3 had a higher performance than the Batch 1 during the first 40,000–50,000 cycles in terms of EDV and capacity (and accordingly lower internal resistance and weight loss), at the end of life they fulfilled only 90,000 cycles. During the tear-down analysis, the visual inspection showed the formation of microshortcircuits across the separator in the upper part of the cells at the end of life. This fact could be explained taking into account the very high

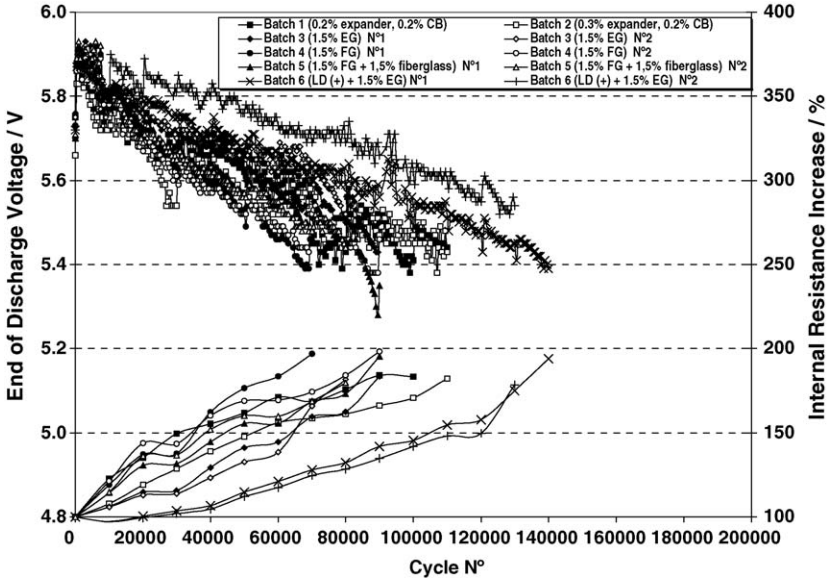

Fig. 10. Number of power assist cycles fulfilled by thermosealed modules (end of discharge voltage and internal resistance vs. cycle no.).

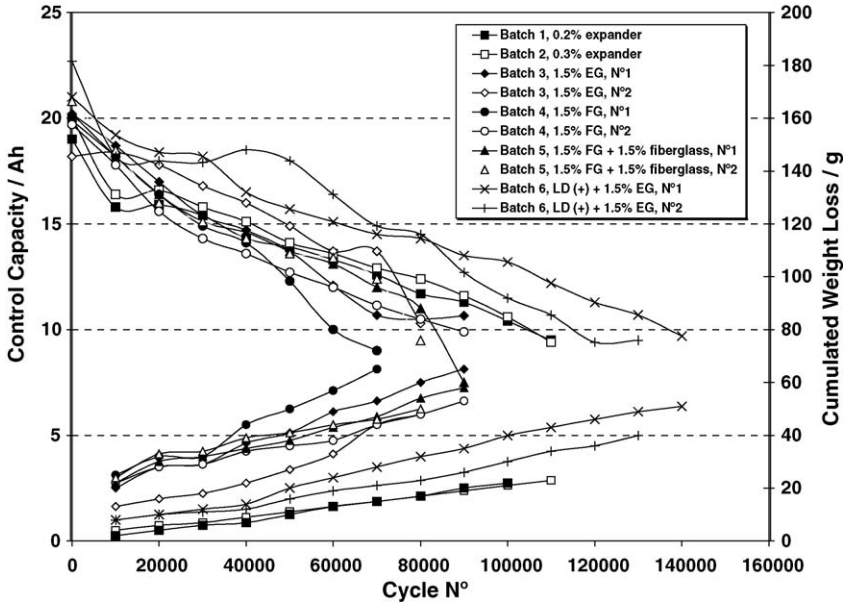

Fig. 11. Number of power assist cycles fulfilled by thermosealed modules (capacity and weight loss vs. cycle no.).

compression found from the beginning, especially in modules belonging to this batch.

With respect to Batches 4 and 5 (both containing flake graphite), in this case they present very similar values in terms of cycle life. This result is also unexpected as in the previous test modules from Batch 4 fulfilled only 40,000 cycles, and in this case reached about 80,000. The explanation can be found in a significantly lower weight loss for FG modules compared to that observed in plugged modules. Microfiberglass in this occasion appears to not significantly influence in cycle life as the modules from Batch 5 have fulfilled as much as 90,000 cycles, although the apparition again of some microshortcircuits (see the sudden fall in EDV curve of battery from Batch 5 in Fig. 10) have shortened somewhat the expected life.

The most significant results is that thermosealed modules containing a higher load of expanded graphite in NAM and with a lower density in PAM have completed 130,000–140,000 power assist cycles (3250–3500 capacity throughput), which represents an increase in cycle life with respect to standard CB formulation in about 20%.

As a general trend, thermosealed modules suffered less weight loss than the corresponding modules with rubber plugs. Fig. 12 shows the capacity and weight loss evolution of four selected batches. Thermosealed battery belonging to Batch 1 has fulfilled 30,000 cycles more than the corresponding rubber

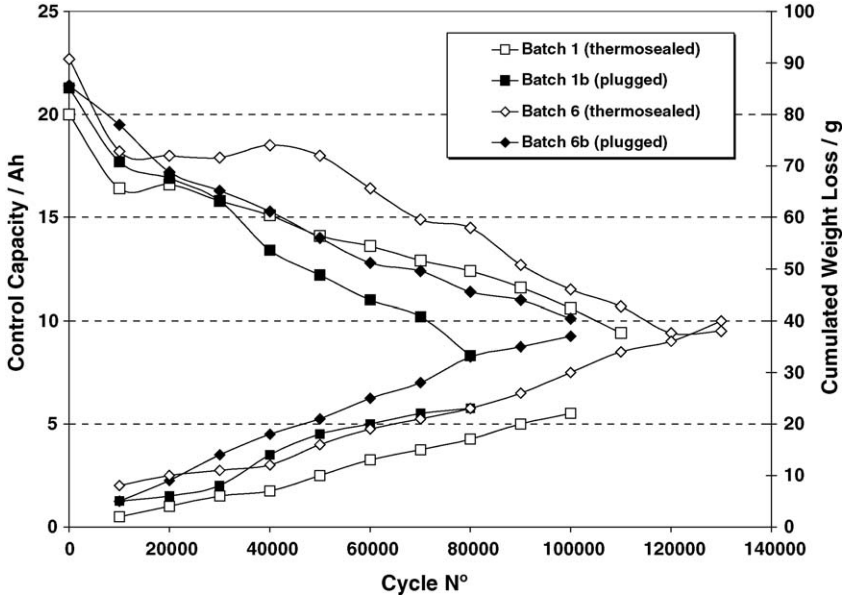

Fig. 12. Cycle life comparison between thermosealed and no thermosealed modules.

sealed module of Batch 1b. This behavior is also observed when cycling performance of batteries belonging to Batches 6 and 6b, both containing expanded graphite, are compared (see Fig. 12).

This could be explained by assuming that the rubber sealing was not very effective during the life in this particular test and therefore gases evolve early [1] under this particular HRPSoC test escaped at lower pressures than the opening valve pressure (fixed at 120 mbar).

Cells from the two differently sealed groups of modules were torn-down for physico-chemical analysis and some 2 V cells were delivered to CSIRO for EPMA analysis. Chemical analysis of the active material samples were carried out using internal procedures based on volumetric (PbO_2) and gravimetric ($PbSO_4$) methods. Active material porosity was measured with a mercury intrusion porosimeter Micromeritics Autopore 9405 and specific surface (BET) with a Micromeritics FlowSorb II 2300.

The most significant chemical data obtained are related to the sulfate distribution at the end of the life, independent of the sealing type as well as of the negative plate formulation of the modules (Table 3), since all the cells analyzed presented very high sulfate content in NAM, mainly located at the upper and middle zones of the plates. This sulfate distribution is consistent with previous results obtained by us from VRLA high power prismatic batteries according to the same power assist profile [5]. With respect to the total amount of sulfate found at the end of the life, "plugged" modules belonging to Batches 3b and 6b, which contain expanded graphite in NAM, showed an overall lower sulfate content (and higher SSA) than the corresponding control (Batch 1b), flake graphite (Batch 4b) and fiber-containing (Batch 5b) prototypes. This indicates the positive influence of this particular carbon type and load in extending cycle life at HRPSoC duty. However, the failed modules belonging to thermosealed Batch 6 which fulfilled 130,000–140,000 cycles had higher sulfate content at the end of the life when compared to standard thermosealed prototypes (Batch 1). The outstanding extension of cycle life in modules with EG could explain the "exhaustion" of NAM leading to more homogeneous sulfate distribution throughout the plates.

Failure mode in this type of HRPSoC duty is therefore ascribed generally to negative plate sulfation as positive plates

Table 3
Tear-down analysis after power assist life cycle test (2.5% DoD at 60% SoC)

Prototype	Positive active material analysis			Negative active material analysis		Number of power assist cycles
	PbO_2 (%)	Porosity (%)	BET ($m^2\ g^{-1}$)	$PbSO_4$ (%)	BET ($m^2\ g^{-1}$)	
Batch 1 (initial)	90.6	48.5	5.1	2.1	0.47	
Batch 1 (control) (thermosealed)	95.5	53.4	1.92	54.2 (top) 50.5 (middle) 15.6 (bottom)	0.26 (top) 0.30 (middle) 0.46 (bottom)	110,000
Batch 1b (control)	95.7	52.2	1.8	68.6 (top) 65.0 (middle) 30.2 (bottom)	0.25 (top) 0.22 (middle) 0.37 (bottom)	80,000
Batch 2 (0.3% exp.) (thermosealed)	95.4	51.4	1.83	53.8 (top) 55.7 (middle) 20.6 (bottom)	0.29 (top) 0.20 (middle) 0.34 (bottom)	110,000
Batch 3 (initial)	88.4	46.2	5.1	5.5	0.60	
Batch 3b (EG)	95.7	50.9	1.72	39.8 (top) 50.2 (middle) 14.9 (bottom)	0.43 (top) 0.36 (middle) 0.52 (bottom)	100,000
Batch 4 (initial)	92.5	47.9	4.0	4.8	0.43	
Batch 4b (FG)	95.4	49.9	3.4	71.3 (top) 48.9 (middle) 23.8 (bottom)	0.40 (top) 0.48 (middle) 0.61 (bottom)	40,000
Batch 5 (initial)	93.0	47.8	4.6	2.1	0.75	
Batch 5b (FG + fiberglass)	95.8	51.8	2.2	54.0 (top) 56.3 (middle) 16.9 (bottom)	0.31 (top) 0.29 (middle) 0.40 (bottom)	90,000
Batch 6 (initial)	93.9	50.6	4.4	2.8	0.59	
Batch 6 (LD + EG) (thermosealed)	94.9	55.9	1.25	56.5 (top) 30.1 (bottom)	0.40 (top) 0.56 (bottom)	140,000
	95.9	57.7	1.38	60.1 (U) 35.5 (L)	0.43 (top) 0.49 (bottom)	130,000
Batch 6b (LD + EG)	95.6	54.0	1.78	47.7 (top) 51.3 (middle) 13.5 (bottom)	0.38 (top) 0.40 (middle) 0.54 (bottom)	100,000

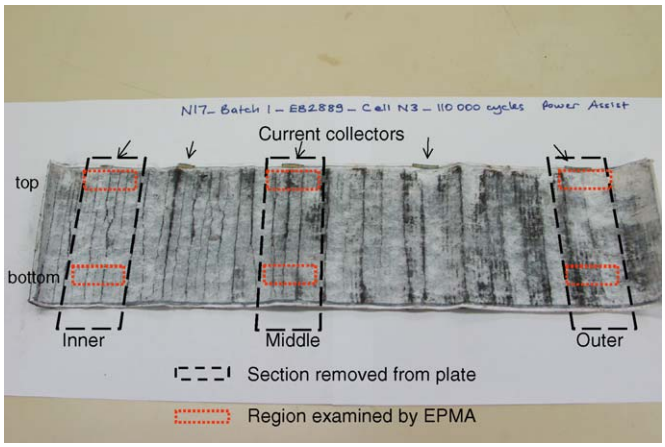

Fig. 13. Sampling of NAM for EPMA analysis.

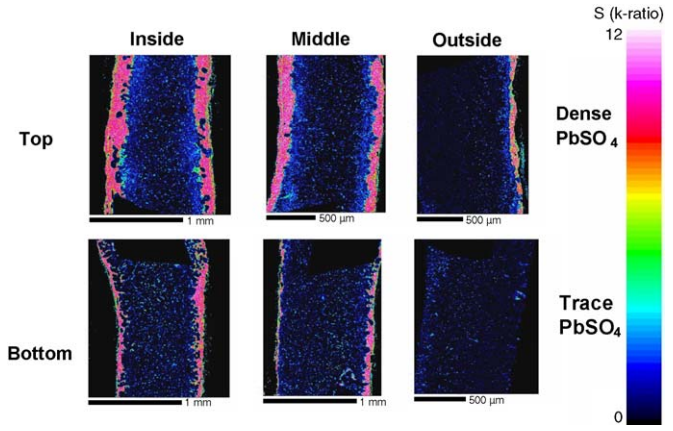

Fig. 14. EPMA data showing concentration of sulfur for the negative plates from a control battery (Batch 1b) after 80,000 power assist cycles.

showed good external appearance during tear-down visual inspection and very high PbO_2 levels (>95%) at the end of life. However, positive active material showed a moderate porosity increase when compared to values obtained after battery formation (from 46–50 to 51–58%), and a remarkable specific surface decrease (from 4.0–5.1 to 1.4–1.9 $m^2\,g^{-1}$) during cycling (Table 3).

CSIRO Energy Technology has prepared samples of negative plate materials, and then conducted electron probe microanalysis (EPMA) so as to characterize the distribution of lead sulfate within the negative plates of each battery type tested. The whole cell-groups (positive plate, negative plate and separator), have been washed free of acid and dried. The negative plate was removed from each cell group and then flattened out in preparation for sampling. The sampling procedure is illustrated in Fig. 13. Vertical strips of each negative plate were excised and then mounted in epoxy resin. From each strip, a section of plate was removed from the top and bottom regions. Each sample was then prepared as a polished cross-section. EPMA data were acquired with a Jeol Model JXA-8900R Superprobe, which was operated at an accelerating voltage of 15 kV and a nominal beam current of 50 nA. The presentation of results is based on the data acquired for sulfur, due to the importance of lead sulfate in the mechanism by which negative plates fail. Information on the abundance of further four elements (lead, oxygen, carbon and calcium) has been used to check that high levels of sulfur actually correspond to high levels of lead sulfate.

Maps of sulfur abundance for negative plates sampled from selected cells of Batches 1 and 6 are presented in Figs. 14 and 15. These samples are taken representative of those from all batches as the pattern of sulfur distribution within each of the negative plates falls within the range set by the results shown in Figs. 14 and 15. In each image, the large portion of the mapped area within the plate that appears completely black is the section of the grid that was included in the analytical (mapped) region. The strips of black along two opposing edges of each image define the exterior of the plate, where bulk electrolyte was present during service. Small irregular shaped regions of black within the plate are voids (pores) that have been exposed in the preparation of the cross-section. The sulfur concentration is rendered in a full-color scale (shown at the right of each image), which typically spans a range of *k*-ratios from 0 to 12. These numbers are treated as approximate values of wt.% S, from which wt.% $PbSO_4$ are calculated. [Pure $PbSO_4$ ideally

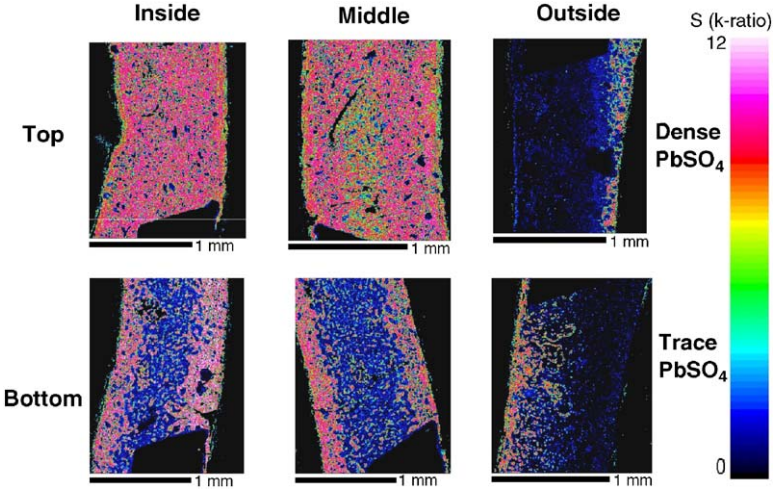

Fig. 15. EPMA data showing concentration of sulfur for the negative plates from a battery of Batch 6b after 100,000 power assist cycles.

should register a *k*-ratio (=wt.% S) of 10.6.] It should be noted that regions which registered the highest concentrations of sulfur are rendered white. The effect of this on the images is that the negative plates for which were recorded the highest abundances of sulfur display light pink bands that extend from the exterior of the plate towards the interior.

As is clear from Figs. 14 and 15, the pattern of sulfur distribution within each of the negative plates is remarkably similar. In summary, the accumulation of lead sulfate has taken place predominantly in the inside portion of each plate, near the center of the spiral cell. For each cross-section, it is observed that the accumulation of lead sulfate occurs preferentially in the surface region of the plate, i.e., closest to bulk electrolyte when the battery was in service. Averaging of the sulfur concentration over the entire mapped area, for these inner regions, yields values which fall in a broad range, from ∼30 to >70 wt.% lead sulfate. Generally, the sample removed from the top of the plate registers significantly higher abundance of lead sulfate. This finding is unusual, although has been previously reported [5] since charge–discharge cycling of lead-acid negative plates normally gives rise to higher concentrations of lead sulfate in the lower part of each plate, due to the combined effects of electrolyte stratification and non-uniform material utilization.

Sulfur maps for the middle portions of the plates (Figs. 14 and 15) returned similar patterns of lead sulfate distribution, for which abundance in the top samples was greater than in the corresponding bottom samples. Averaged concentrations of lead sulfate were generally lower than those recorded for the inner portions of the respective plates.

On moving to the outside of the plate (i.e., to the end of the spiral, which is the portion of the plate closest to the cell container wall), a substantial fall in the levels of sulfur has been noted which is consistent with little participation of the outer portion of the plate in charge–discharge.

For each plate examined, the abundance of lead sulfate in both outer samples (top and bottom) is not far above background concentration.

To illustrate the extent to which the distribution of lead sulfate in negative plates changes during this form of HRPSoC duty, sulfur maps have been recorded for plates from a cell that was removed from service immediately prior to the commencement of the power assist profile. Fig. 16 shows EPMA sulfur maps for a negative plate that was discharged to 60% SoC, removed from the cell, and then prepared quickly for analysis. The six locations are the same as those used in all previous samples. From examination of the sulfur maps, it is noted that the initial discharge, prior to HRPSoC service, produces a uniform distribution of lead sulfate (25–30%). The uniformity is defined both along the plate (from inside to outside) and across the plate (from interior to the surface, closest to bulk electrolyte). Overall, it is clear that HRPSoC duty is responsible for the gross redistribution and accumulation of lead sulfate that has taken place in each of the plates that has been examined to date.

Up to date, it had been found by CSIRO and complemented by our group in previous studies on prismatic design cells [1,5], that negative plates under PSoC duty developed lead sulfate mainly on the surfaces of NAM, and that sulfate accumulates predominantly in the upper part of negative electrodes. However, this work has shown that, due to the cylindrical cell design of these 6 V modules, a novel and remarkably consistent pattern develops within each variety of negative plate (from inside to outside). Given that service life of these cells is limited by that of the negative plate, and that this type of accumulation of lead sulfate has been shown to be the cause of cell failure under other similar forms of PSoC duty, it is clear that the substantial changes in both the overall concentration and distribution of lead sulfate are primarily responsible for the failure of the cells.

Trying to explain this selective accumulation of sulfate in negative plates of spiral configuration, a complementary temperature study has been performed by placing several thermocouples in different cell zones, i.e., from the top to the bottom as well as inside and outside of the cell of a 6 V prototype belonging to Batch 6. This study has been carried out due to the evidence that the highest levels of lead sulfate correspond to the hottest part of the cell (center/inside-top). The higher temperature might

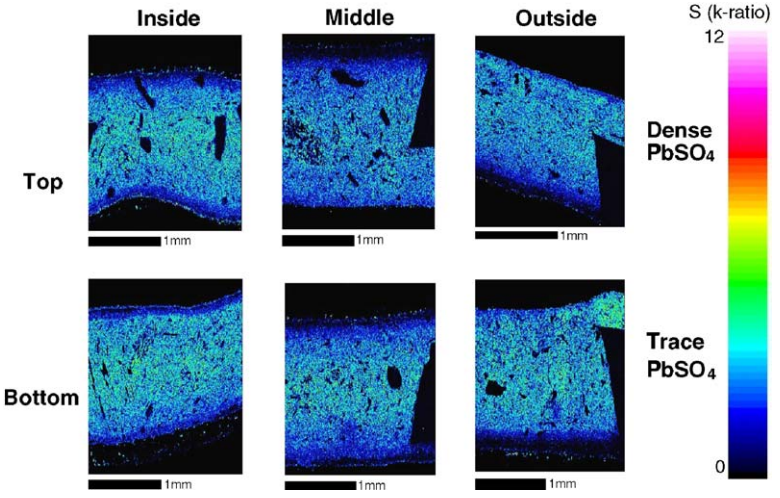

Fig. 16. EPMA data showing concentration of sulfur for the negative plate from an uncycled battery (Batch 6) that has been discharged to 60% SoC prior to removal for analysis.

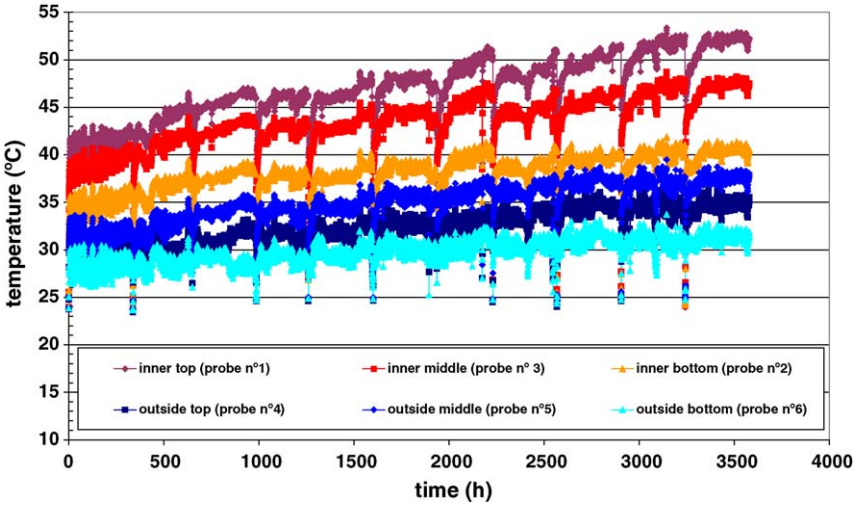

Fig. 17. Temperature evolution in different parts of central cell of a 6 V module along HRPSoC cycle life.

accelerate the accumulation of lead sulfate by enhancing the evolution of hydrogen. A second process that warrants consideration is oxygen recombination and how it is affected by temperature. The generally accepted view is that the recombination proceeds more rapidly as temperature increases. Given that the product of recombination is lead sulfate, then this may provide a direct explanation for the greater accumulation of lead sulfate in the hottest part of the negative electrodes.

As can be seen in Fig. 17, there is a temperature gradient from the beginning of cycling which depends on the thermocouple location. The hottest part corresponds to the top-middle/inside of the cell. This zone is the closest to the current collectors and additionally, the oxygen recombination is produced predominantly there, due to progressive drying-out of the separator. As the HRPSoC cycling proceeds, the temperature rise is higher for the top and middle inner parts of the cell (>10 °C increase from the beginning to the battery failure), whereas temperature rise in bottom/inside zone of the cell as well as the outer parts of the cell is about 5 °C along the cycle life test. The whole of the data recorded suggest a direct relationship between lead sulfate concentration determined by both chemical and EPMA analysis and temperature.

4. Conclusions

Six volt AGM VRLA prototypes with spirally wound cells and including novel carbon and fiberglass additives in NAM formulation have been manufactured and electrically tested. The special cylindrical cell design has allowed an excellent performance in terms of high power capability and HRPSoC duty. Furthermore, the addition of conductive expanded graphite has improved charge acceptance and cycle life with respect to the other formulations (20–25% compared to control batch containing standard load and type of carbon black). However, the use of flake graphite has been detrimental for cycle life due to its lower surface area. On the other hand, the use of micro-fiberglass in NAM increases the NAM surface area, although the effect on cycle life is still unclear (cycle life in rubber sealed 6 V modules has increased but not in thermosealed ones). The prototypes in which the amount of organic expander has been varied have shown the same number of HEV cycles fulfilled, indicating that the load of organic expander in NAM has an influence in charge acceptance but not on the cycle life at PSoC.

Finally, the best combination of initial performance and cycle life at PSoC is obtained, respectively, with a lower PAM density and adding expanded graphite to NAM that improves active material conductivity along life.

The failure mode under HRPSoC is best described as irreversible sulfation of NAM that leads to an early evolution of hydrogen under high rate charging. In this way, we have found that thermosealed modules have a longer HEV life than the no thermosealed counterparts since water loss has a significant influence in this type of PSoC duty.

The special spiral design of these 6 V modules has allowed the development of a new pattern of lead sulfate distribution from inside to outside of unrolled negative plates, apart from the patterns already described from surface-to-interior/top-to-bottom of the plates. We have demonstrated that the utilization of active mass and the accumulation of lead sulfate in the negative plates is directly related to the temperature profile that develops in the cell as the PSoC cycling progresses, i.e., the hottest parts of the cell correspond to the highest sulfate content found at the end of life. Additionally, as the PSoC duty proceeds, the drying-out of the separator increases the amount of the oxygen that reaches the negative plate, enhancing the level of oxygen recombination. Since recombination proceeds more rapidly as temperature increases and given that the product of recombination is lead sulfate, then this may provide a direct explanation for the greater accumulation of lead sulfate in the hottest part of the negative plate.

Acknowledgements

This work has been supported by the Advanced Lead-Acid Battery Consortium, Research Triangle Park, NC, USA. Our acknowledgement also to Tony Ferreira (Hollingsworth & Vose)

and Mathis Wissler (Superior Graphite) for the supply of the fiberglass and expanded graphite, respectively.

References

[1] L.T. Lam, N.P. Haigh, C.G. Phyland, A.J. Urban, J. Power Sources 133 (2004) 126–134.
[2] A.F. Hollenkamp, W.G.A. Baldsing, S. Lau, O.V. Lim, R.H. Newnham, D.A.J. Rand, J.M. Rosalie, D.G. Vella, L.H. Vu, Overcoming Negative-Plate Capacity Loss in VRLA Batteries Cycled Under Partial State-of-Charge Duty, ALABC Project N1.2 Final Report, July 2000–June 2002.
[3] F. Trinidad, C. Gimeno, J. Gutiérrez, R. Ruiz, J. Sainz, J. Valenciano, J. Power Sources 116 (2003) 128–140.
[4] A. Cooper, J. Power Sources 133 (2004) 116–125.
[5] M.L. Soria, J.C. Hernández, J. Valenciano, A. Sánchez, F. Trinidad, J. Power Sources 144 (2005) 473–485.
[6] A. Ferreira, J. Jordan, J. Wertz, G. Ziguris, J. Power Sources 113 (2004) 39–46.
[7] EUCAR Traction Battery Working Group;
(a) Specification of test procedures for hybrid electric vehicle traction batteries, September 1998;
(b) Specification of test procedures for energy storage of 42 V-vehicle applications, August 2003.
[8] R.H. Newnham, W.G.A. Baldsing, A.F. Hollenkamp, O.V. Lim, C.G. Phyland, D.A.J. Rand, J.M. Rosalie, D.G. Vella, Advancement of Valve-Regulated Lead-Acid Battery Technology for Hybrid-Electric and Electric Vehicles, ALABC Project C/N1.1 Final Report, July 2000–June 2002.